analytical chemistry

Article

pubs.acs.org/ac

Amyloid-β-Secondary Structure Distribution in Cerebrospinal Fluid and Blood Measured by an Immuno-Infrared-Sensor: A Biomarker Candidate for Alzheimer's Disease

Andreas Nabers,[†] Julian Ollesch,[†] Jonas Schartner,[†] Carsten Kötting,[†] Just Genius,[‡] Henning Hafermann,[‡] Hans Klafki,[§] Klaus Gerwert,[*,†] and Jens Wiltfang[‡,§,∥,⊥]

[†]Department of Biophysics, Ruhr-University Bochum, 44780 Bochum, Germany

[‡]Clinics for Psychiatry and Psychotherapy, LVR-Clinical Center Essen, 45147 Essen, Germany

[§]Department of Psychiatry and Psychotherapy, Georg-August-University Göttingen, University Medical Center, 37099 Göttingen, Germany

[∥]German Center for Neurodegenerative Diseases (DZNE), 37099 Göttingen, Germany

Supporting Information

ABSTRACT: The misfolding of the Amyloid-beta (Aβ) peptide into β-sheet enriched conformations was proposed as an early event in Alzheimer's Disease (AD). Here, the Aβ peptide secondary structure distribution in cerebrospinal fluid (CSF) and blood plasma of 141 patients was measured with an immuno-infrared-sensor. The sensor detected the amide I band, which reflects the overall secondary structure distribution of all Aβ peptides extracted from the body fluid. We observed a significant downshift of the amide I band frequency of Aβ peptides in Dementia Alzheimer type (DAT) patients, which indicated an overall shift to β-sheet. The secondary structure distribution of all Aβ peptides provides a better marker for DAT detection than a single Aβ misfold or the concentration of a specific oligomer. The discrimination between DAT and disease control patients according to the amide I frequency was in excellent agreement with the clinical diagnosis (accuracy 90% for CSF and 84% for blood). The amide I band maximum above or below the decisive marker frequency appears as a novel spectral biomarker candidate of AD. Additionally, a preliminary proof-of-concept study indicated an amide I band shift below the marker band already in patients with mild cognitive impairment due to AD. The presented immuno-IR-sensor method represents a promising, simple, robust, and label-free diagnostic tool for CSF and blood analysis.

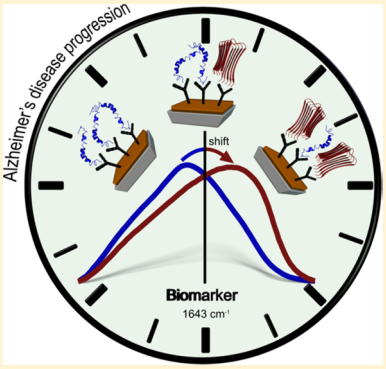

Alzheimer's disease (AD) is the most common cause of dementia and affects over 35 million individuals worldwide. Clinical and research evidence indicates that the neuropathology starts 10−20 years before AD becomes clinically overt.[1−4] The amyloid cascade hypothesis postulates[5] that misfolding and subsequent aggregation of Aβ peptides is responsible for neurodegeneration. However, it is an ongoing discussion, whether Aβ aggregation is the cause or epiphenomenon of AD.[6] Nevertheless, aggregation of Aβ peptides into neurotoxic soluble oligomeric species and finally into insoluble fibrillar structures is associated with AD.[7,8] Thus, misfolding precedes or accompanies aggregation.

Widely accepted criteria for the clinical diagnosis of Alzheimer's disease were published by the National Institute of Neurological and Communicative Disorders and Stroke (NINCDS) and the Alzheimer's Disease and Related Disorders Association (ADRDA) in 1984.[9,10] Updated and revised diagnostic guidelines were elaborated 2007−2011.[11−15] The two most important differences to the original NINCDS-ADRDA criteria were (i) the definition of three phases of the disease: preclinical, symptomatic predementia (mild cognitive impairment due to AD, MCI-AD), and dementia due to AD (DAT = Dementia Alzheimer type) and (ii) the incorporation of biomarkers of Aβ accumulation and biomarkers of neurodegeneration or injury.[12] Of particular clinical relevance for the development of therapies is the reliable identification of preclinical or predementia stages and the clear distinction between DAT and other forms of dementia premortem.[16] Even today, a definite AD diagnosis can only be given post-mortem. However, the performance of current diagnostic tools for early stages is limited[17−19] and novel diagnostic biomarker candidates[20−22] remain inadequate or have not fully entered clinical routine yet.[14,15,23] In this context, several biomarker studies have shown that Aβ-aggregates are rich in β-sheets,[24−28] as compared to the unfolded or partially α-helical individual peptides. Additionally, the presence of individual oligomeric Aβ species in CSF and blood was described, but the concentration of these species itself may not correlate with early stages of AD.[29−31] Here, we present the application of a novel immuno-

Received: November 11, 2015
Accepted: February 1, 2016
Published: February 1, 2016

DOI: 10.1021/acs.analchem.5b04286
Anal. Chem. 2016, 88, 2755−2762

infrared-sensor (Figure 1),[32] which monitors the secondary structure distribution of all Aβ states extracted from CSF and blood, especially its α-helix and β-sheet secondary structure distribution.

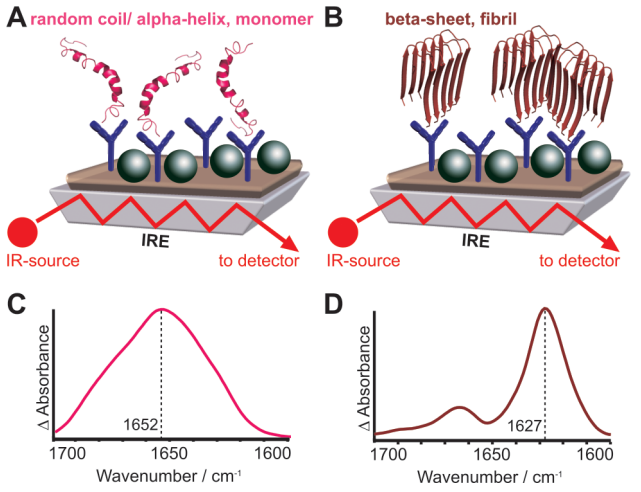

Figure 1. Schematic representation of the immuno-ATR-FT-IR-spectroscopic setup. The IR-beam is totally reflected in the IRE multiple times (A, B) generating an evanescent wave at the boundary layer. Thus, tethered antibodies capture Aβ peptides out of liquid samples in the evanescent wave for detection of the infrared absorbance (C, D). The scheme exemplarily depicts the detection of monomerized (A, C) and fibrillized (B, D) synthetic Aβ1-42 conformations drawn from PDB entries 1Z0Q and 2BEG. The amide I bands clearly exhibit a β-sheet-induced band shift in the fibrillized sample (D).

For the analysis of the secondary structure distribution of peptides and proteins, Fourier transform-infrared (FT-IR) spectroscopy is an excellent tool.[33] Secondary structure analysis of proteins associated with neurodegenerative disorders has already been performed on purified, isolated proteins.[34−37] In these studies, the infrared amide I absorbance band between 1700 and 1600 cm^{-1} was analyzed. The amide I band originates from the protein backbone C═O stretching vibration. Its frequency depends on the respective secondary structure.

In our study, an immuno-IR-sensor[32] was applied to complex body fluids. Briefly, an antibody is attached to the surface of the internal reflection element of a flow-through attenuated total reflection (ATR) setup to extract Aβ peptides out of the body fluid. Thereby, the secondary structure distribution of the surface attached Aβ peptides from CSF and blood plasma was measured without further purification or concentration. A sufficient signal/noise ratio of the amide I band of Aβ extracted from CSF or blood plasma was achieved.

The immuno-IR-sensor indicated that the overall Aβ secondary structure distribution was shifted mostly toward the misfolded β-sheet in DAT patients. Thus, the amide I band frequency above or below a decisive spectral marker frequency was used to discriminate between DAT and disease control (DC) patients. By analyzing 99 CSF samples, we observed a sensitivity of 94% and a specificity of 88%, whereas an analysis of 86 blood samples resulted in a sensitivity of 75% and a specificity of 88%. The CSF results were validated with an additional set of patient samples. An accuracy of 90%, sensitivity of 88%, and specificity of 93% were determined.

As compared to conventional ELISA tests, the sensor has the advantage to monitor not the concentration of a single Aβ folding state or of selected oligomers, but the overall distribution of the Aβ fraction in CSF and blood. Thereby, the secondary structure distribution of all soluble Aβ forms is detected in the amide I band as an averaged signal. We propose this average distribution as an easily accessible, novel biomarker candidate for DAT and potentially for MCI-AD.

EXPERIMENTAL SECTION

The prospective study fulfills the international standards for studies of diagnostic test accuracy in dementia.[38]

Patient Cohorts and Clinical Phenotyping. The patient cohort was divided into three subgroups, probable dementia due to Alzheimer's disease (Dementia Alzheimer type, DAT), mild cognitive impairment due to AD (MCI-AD), and disease controls (DC). The DC group comprised patients with dementia of other origin and nondemented patients with heterogonous neurological or psychiatric diseases but without memory complaints. Patients with probable dementia due to Alzheimer's Disease (DAT, n = 33), MCI-AD (n = 11), and disease controls (DC, n = 66) were admitted to the gerontopsychiatric unit of the department of psychiatry and psychotherapy, LVR Clinics, University of Duisburg-Essen, for dementia diagnostics from 07/2009 to 12/2013. CSF and blood samples were collected and stored at one clinical center adhering to one standard operation procedure to minimize storage and sampling handling artifacts. The patient cohort consisted of 46 male (10 DAT, 33 DC and 3 MCI-AD, mean age 67 ± 11 years) and 64 female (23 DAT, 33 DC, and 8 MCI-AD, mean age 70 ± 12) patients, as summarized in Table S-1A. Clinical diagnosis of DAT was made according to the criteria of the National Institute for Neurological and Communicative Disorders and Stroke and the Alzheimer's Disease and Related Disorders Association (NINCDS-ADRDA).[9−15,39] The majority of patients with DAT presented with early AD (18/33) and 10 patients were seen within a moderate clinical disease stage. Diagnosis of MCI-AD was performed according to the 2011 recommendations from the National Institute on Aging.[15] Memory complaints in MCI patients had to be associated with a performance in the mini mental state examination test (MMSE) and a minimum of 25 MMSE test score, preserved activities of daily living, and a CSF biomarker pattern (elevated phospho-Tau/total-Tau and decreased Aβ peptide ratio 1-42/1-40) indicating the AD predementia stage. The clinical diagnosis of DC was performed according to the International Classification of Diseases (ICD-10). The DC cohort included patients without dementia and patients with schizophrenia, bipolar disorders, depression, and dementia not due to AD. The diagnosis of DC patients was cross validated by their CSF dementia biomarker and neuroimaging panel, that is patients with a biomarker signature indicating DAT (decreased Aβ peptide ratio 1-42/1-40 and/or neuroimaging) were excluded. Standardized clinical assessment was conducted by gerontopsychiatrists and neuropsychologists within the setting of an University Memory Clinic, and the clinical diagnosis was independently validated by an expert gerontopsychiatrist (JW). Gerontopsychiatrists and neuropsychologists had access to all available clinical, neuroimaging, psychometric, and conventional CSF dementia biomarker data but were blinded for the FT-IR-analysis results. Patients were investigated by psychometric testing (mini mental state examination, MMSE, and/or extended neuropsychological

DOI: 10.1021/acs.analchem.5b04286
Anal. Chem. 2016, 88, 2755−2762

evaluation) and CSF-guided neurochemical dementia diagnostics (CSF-NDD). For a subset of patients, in addition, neuroimaging (cranial computed tomography or 3 T magnetic resonance imaging) data were available. For some patients the complete set of diagnostic measures could not be performed (for details see Table S-2). The standard operating procedures for sampling of lumbar CSF and EDTA-blood plasma (sample taking, preanalytical sample handling, biomaterial banking, shipment) followed the guidelines of the German Competence Net Dementias.[40] CSF-concentrations of Aβ1-42, Aβ1-40, total-Tau (ttau), and phospho-Tau181 (ptau) were measured in duplicate by commercially available ELISA in an accredited expert laboratory for CSF-NDD (P. Lewczuk, University of Erlangen-Nürnberg, Germany).[41,42] Since not for every single patient the CSF Aβ peptide concentration ratio Aβ(1-42/1-40) as determined by the Erlangen laboratory was available (compare Table S-2), all CSF samples were additionally assessed with the MSD V-Plex Aβ peptide panel multiplex kit employing monoclonal antibody 6E10 for detection (Meso-Scale Discovery, Rockville MD). The Aβ peptides Aβ38, 40, 42 were determined according to the manufacturer's instructions after 16-fold dilution of the CSF samples with "Diluent 35" (MSD). The Aβ42/40 ratios calculated from the multiplex-assay data were in good agreement with the CSF-NDD ELISA data (Spearman $r = 0.81$, $p < 0.001$, 80 pairs). Table S-2 summarizes the clinical, psychometric (MMSE) and CSF biomarker phenotyping data of the patient collective, including cutoff values, mean, standard deviation, and MIN-MAX values for MMSE and the CSF dementia biomarkers.

The study was approved by the ethical board of the University of Duisburg-Essen (ID 12 5160 BO) and the research use of the samples and data was in accord with the terms of the informed consents.

From continued patient recruitment within the study, CSF samples of 31 similarly well-characterized patients (14 DC, 17 DAT) were available. Age and gender matched well with the main cohort (Table S-1B). These samples were used as additional validation set.

Workflow. For the FT-IR-spectroscopic analysis of Aβ peptides present in body fluids, our published protocol[32] had to be slightly optimized.

Briefly, a Vertex 70 V FT-IR-spectrometer (Bruker, Ettlingen, Germany) with external MIR-source, equipped with a 24 h lN2-cooled MCT-detector and a vertical variable angle ATR-setup (Specac, Orpington, U.K.), with a trapezoid Ge-crystal (52 mm × 20 mm × 2 mm, Korth Kristalle, Altenholz, Germany) as an internal reflection element was used (see Figure S-1 for a schematic drawing).

The total volume of the flow-cell including all connection tubes was reduced to 450 μL. Thus, the volume dependent concentration sensitivity for Aβ was optimized. For each analysis, one sensor element per sample was functionalized with silane-monolayers[43] and antibodies were covalently attached. The surface was blocked with casein to generate an inert surface against other CSF and blood components. Within our optimized method, the monoclonal antibody A8978 (Sigma-Aldrich, aa13-28) was used instead of 1E8, which had been applied in the original protocol[32] for Aβ capturing. For the analysis, 50 μL of CSF or 150 μL of EDTA-blood plasma were thawed immediately before analysis and added to the circulating buffer, respectively. The flow-rate was set to 1 mL/min. All procedural steps needed 4 h in total.

Bioinformatics. Data evaluation and statistic tests were performed using both built-in and in-house procedures programmed with Matlab 2012A (Mathworks) and Origin 2015 (Origin Laboratories). Data distribution was analyzed with nonparametric Kruskal–Wallis analysis of variance (ANOVA) and Spearman-rank-correlation. The spectral classifying marker frequency for DC and DAT differentiation was determined by receiver operator characteristics (ROC)-curve analysis. The performance of the marker band was tested in repeated cross-validations. The amide I maximum of eight randomly selected patients per class (out of the total patient collective) was used for training. The marker band was scanned from 1630.5 to 1659.5 cm^{-1}, and at each wavenumber the accuracy, sensitivity, and specificity was determined. This step was repeated 30 times. The reliability of the determined marker frequency of each training cycle was verified by cross-validation with the remaining test-data set.

Fluorescence Microscopic Analysis. Fluorescence microscopy was performed as described[32] with optimizations given in the Supporting Information.

RESULTS AND DISCUSSION

Analysis of Aβ Peptide Secondary Structure in Body Fluids. For the present analysis, our sensor was functionalized with antibody A8978 recognizing a core epitope of Aβ peptides (aa Aβ13-28) to extract all Aβ variants at the same time (Figure 1A,B). All preparative steps were highly reproducible and controlled by corresponding infrared spectra. Neither albumin (HSA), nor IgG2, nor α-synuclein bound unspecifically to the sensor surface (Figure S-2). In addition, Aβ binding was confirmed with fluorescence-labeled antibody 1E8 (Figure S-3). No induction of specific secondary structures was observed during Aβ binding to the antibody (Figure S-4 and Nabers, Ollesch et al.[32]). Hence, neither A8978 nor 1E8 were selective for a specific secondary structure (Figure S-5 and Nabers, Ollesch et al.[32]).

α-Helical and random coil monomeric synthetic Aβ1-42 or β-sheet rich fibrillary synthetic Aβ1-42 peptide bands showed the characteristic amide I bands at 1652 cm^{-1} for α-helix and 1627 cm^{-1} for the β-sheet, respectively (Figure 1C,D). Purified monomeric, oligomeric, and prefibrillar preparations of synthetic Aβ1-42 and Aβ1-40 could be easily distinguished by their characteristic amide I band (Figure S-5A–D). In contrast, the overall amide I band of Aβ extracted out of CSF or blood plasma reflects the overall distribution of secondary structures of all Aβ peptide variants present in the sample. For instance, scaled linear in silico combinations of different secondary structure distributions illustrated an amide I band shift to lower wavenumbers by increasing the β-sheet content (Figure S-5E). This effect became more evident by adding synthetic fibrillar Aβ (1 ng/mL) to the sensor-surface immobilized Aβ fraction extracted from CSF of a DC patient. As a result, fibrillar Aβ attached to the antibody layer and contributed to the overall amide I band. Consequently, the amide I band of Aβ shifted from 1648 to 1641 cm^{-1} (Figure S-6). The combination of immunological specificity of the ATR surface with an ATR flow-through system provides the amide I absorbance band of the extracted Aβ fraction with a sufficient signal/noise ratio under physiological and nondenaturing sample conditions.[32] In summary, the applied sensor monitors the overall secondary structure distribution of the total Aβ peptide fraction extracted from CSF and blood.

DOI: 10.1021/acs.analchem.5b04286
Anal. Chem. 2016, 88, 2755–2762

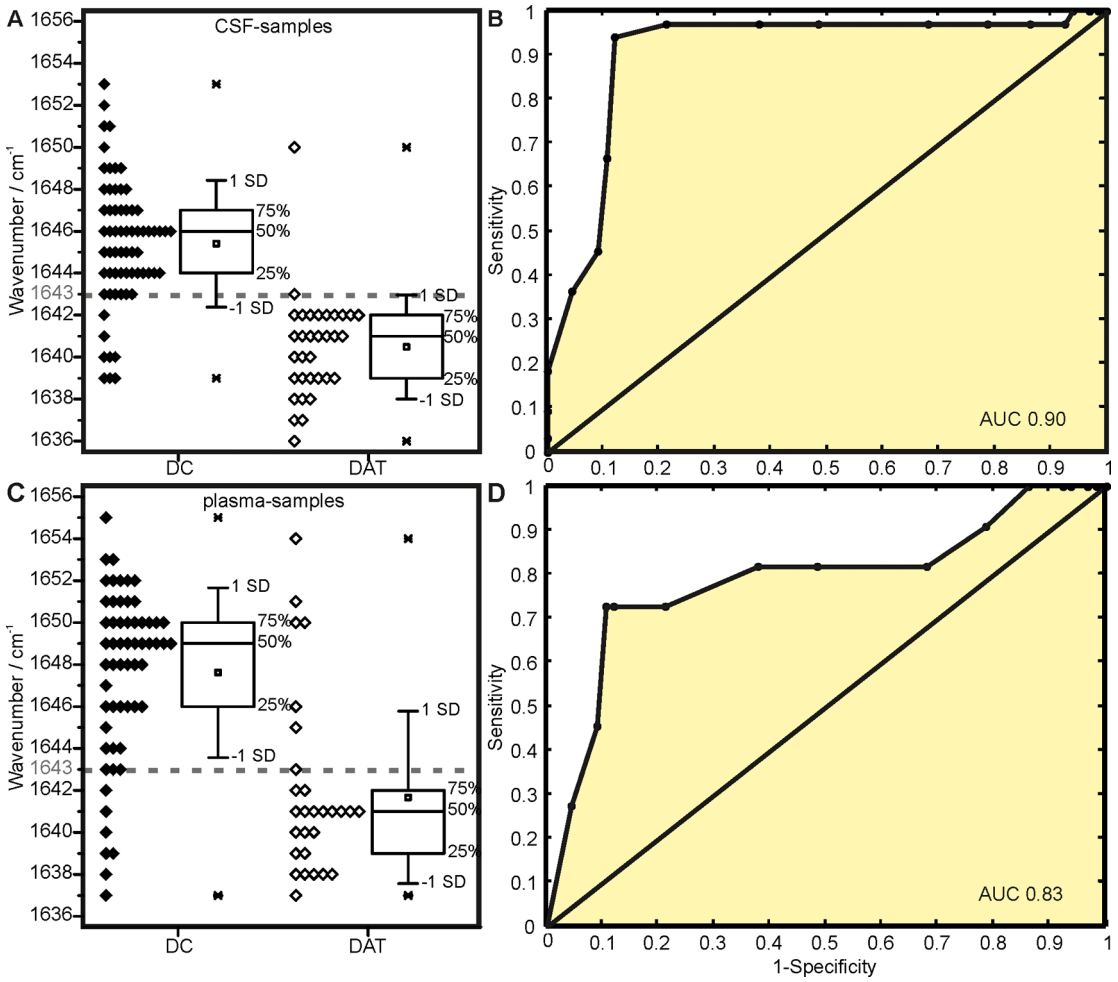

Figure 2. Distributions of the amide I maximum frequencies as recorded of CSF (A) and blood plasma (C) indicate a clearly separable spectral downshift associated with DAT. A marker band at 1643 cm^{-1} separates controls with 90% (A) and 84% accuracy (C, dashed lines). Solid diamonds depict DC patient samples and empty diamonds DAT cases. 25/50/75% quantiles are displayed in box-plots as horizontal lines, the average band position (square), ± standard deviation (whiskers), and observed minimum/maximum values (×) are displayed. A ROC curve was obtained by variation of the marker frequency (B, D). AUCs of 0.90 and 0.83 were achieved with CSF and blood plasma samples, respectively.

Spectral Discrimination of DAT and DC Patients Based on CSF. In Figure 2A, the amide I frequencies of DC and DAT patients are shown. DAT patients exhibited a significantly lower average amide I band maximum position as compared to the DC group ($p < 0.0001$). The average amide I maximum was 1645 ± 3 cm^{-1}, with a median value of 1646 cm^{-1} for the DC group. The 25−75% percentiles were between 1644 and 1647 cm^{-1}. The average amide I maximum of DAT patients was downshifted to 1640 ± 3 cm^{-1} with a median of 1641 cm^{-1}. The 25−75% percentiles were between 1639 and 1642 cm^{-1} (Figure 2A). The amide I positions of the CSF samples did not show a Gaussian normal distribution. Therefore, we used the nonparametric Kruskal−Wallis analysis of variance to indicate a significant difference of the distributions to a confidence level of 0.05. The signal downshift indicates an accumulation of β-sheet structures of aggregated Aβ conformations in CSF of DAT patients. The amide I band above or below a marker band can be used for the discrimination between DC and DAT. The classifying marker frequency was determined by 30 iterative ROC-curve analyses of 30 randomly selected eight vs eight DC/DAT training-data sets out of the total patient collective (details see methods). Each repetition on the training-data sets yielded a best discriminating marker frequency value for maximal accuracy. This frequency was consistently determined at 1643 cm^{-1}. Thus, a robust and simple marker band for DC/DAT discrimination was determined. ROC curve analysis of the total patient collective indicated an area under the curve (AUC) of 0.90 (Figure 2B) with a maximum accuracy consistent at 1643 cm^{-1}. Assigning every patient with an amide I band maximum frequency <1643 cm^{-1} as DAT patient, an accuracy of 90%, a sensitivity of 94%, and a specificity of 88% was achieved for CSF samples, with regard to the clinical diagnosis (Table 2A). Thus, an accurate discrimination between the two diagnostic groups was achieved. Only 2 out of 33 clinical DAT patients were falsely assigned negative, and only 8 out of 66 control patients were falsely assigned positive.

Additionally, the identified marker band criterion, amide I frequency <1643 cm^{-1} denotes DAT, was validated using an independent data set of 31 patients not included into the main analysis. Thus, 14 DC and 17 DAT patients were discriminated with an accuracy of 90%, sensitivity of 88%, and specificity of 93%. In the next step we compared the amide I band frequency with other clinically established markers as the CSF concentrations of Aβ1-42 (Figure S-7A), ptau ($r = -0.57$, $p = 1.3 \times 10^{-10}$, Figure S-7C), and ttau ($r = -0.54$, $p = 1.2 \times$

DOI: 10.1021/acs.analchem.5b04286
Anal. Chem. 2016, 88, 2755−2762

10^{-9}, Figure S-7D) and with the Aβ42/40 ratios as determined with two assays ($r = 0.58$, $p = 2.1 \times 10^{-8}$ (ELISA) and $r = 0.58$, $p = 2.0 \times 10^{-11}$ (MSD), Figure S-7B and Table 1).

Table 1. Summary of the Spearman Rank Correlation (r_S) and the Significance Value (p Value for a Niveau of $\alpha = 0.05$) between the Amide I Maximum Positions and Neurochemical Biomarkers of CSF Samples

	vs	r_S	p value
amide I maximum	MMSE	0.2427	0.0204
	Aβ1-42	0.4476	1.3×10^{-6}
	Aβ1-40	−0.1627	0.1416
	Aβ1-42/Aβ1-40 ratio (ELISA, Erlangen lab)	0.5771	2.1×10^{-8}
	Aβ1-42/Aβ1-40 ratio (mesoscale)	0.5844	2.0×10^{-11}
	ptau	−0.5714	1.3×10^{-10}
	ttau	−0.5462	1.2×10^{-9}
	age	−0.0604	0.5307

The Spearman correlations indicate that a higher CSF concentration of ptau, ttau (both are considered biomarkers of neuronal destruction), or the decreased Aβ42/40 ratio is accompanied by the amide I band downshift (Table 1, Figure S-7). The amide I maximum frequency of Aβ did not correlate with the age of participants or the Aβ1-40 CSF-concentration (Table 1).

Spectral Discrimination of DAT and DC Patients Based on EDTA-Blood Plasma. Next, we applied the novel infrared-sensor to the analysis of EDTA-blood plasma, which is more easily accessible than CSF. Within the study, samples of 28 DAT and 58 DC patients were available. The DC group showed an average amide I maximum of 1647 ± 4 cm^{-1} (median 1649 cm^{-1}), whereas the average maximum of the DAT group was significantly downshifted to 1642 ± 4 cm^{-1} (median 1641 cm^{-1}, $p < 0.0001$, Figure 2C). Again, the amide I positions of the plasma samples did not show a Gaussian normal distribution, but the nonparametric Kruskal–Wallis analysis of variance indicated a significant difference of the distributions to confidence level 0.05. The identical marker frequency classifier as used before (<1643 cm^{-1}) was determined by a randomized 30-times repeated 8 + 8 versus 76 patient cross validation, performed as described. It resulted in a discrimination of the diagnostic groups with an accuracy of 85%, a sensitivity of 75% and a specificity of 88%. Thus, only 7 false positive of 58 DC patients and 7 false negative of 28 participants with DAT were falsely classified. ROC analysis yielded an AUC of 0.83 (Figure 2D). In comparison to the analysis of Aβ from CSF, the accuracy and sensitivity were lower in blood.

Discrimination of DC and MCI-AD Patients. In the next step we investigated the capability of the method to identify AD patients in the MCI-stage (MCI-AD). However, because of a comparatively small number of patients with MCI-AD ($n = 11$) our data have to be regarded as a preliminary proof-of-concept study. We analyzed CSF and plasma of 11 MCI-AD patients. As explained above, the MCI-AD patients presented elevated tau and decreased Aβ1-42 levels in CSF, indicating incipient Alzheimer's disease.

The median Aβ amide I band recorded from MCI-AD CSF samples exhibited a downshift below the same 1643 cm^{-1} marker band as shown for DAT patients (Figure 3). A total of 8 out of 11 MCI-AD patients were correctly classified by our sensor. Three of the MCI-AD patients exhibited an amide I frequency >1643 cm^{-1} and thus appear to be "false negative". MCI-AD patients yielded an average amide I maximum at 1642 ± 3 cm^{-1} (below the marker band), with the median identical to the DAT group at 1641 cm^{-1} (Figure 3A).

Box-plots indicate that the MCI-AD and DC group (same as Figure 2A,C) statistically significantly differ in the amide I band distributions ($p < 0.005$). The marker frequency criterion of the amide I maximum below 1643 cm^{-1}, an accuracy of 86%, sensitivity of 73%, and a specificity of 88% was reached for the discrimination of MCI-AD patients from the DC based on CSF (Table 2B). ROC analysis yielded an AUC of 0.79 (Figure 3B).

We further analyzed EDTA-blood plasma of MCI-AD patients. Again, the Aβ amide I bands showed downshifts below 1643 cm^{-1} for 5 out of 10 patients. Box-plots comparing the amide I maxima of MCI-AD and DC patients indicate a

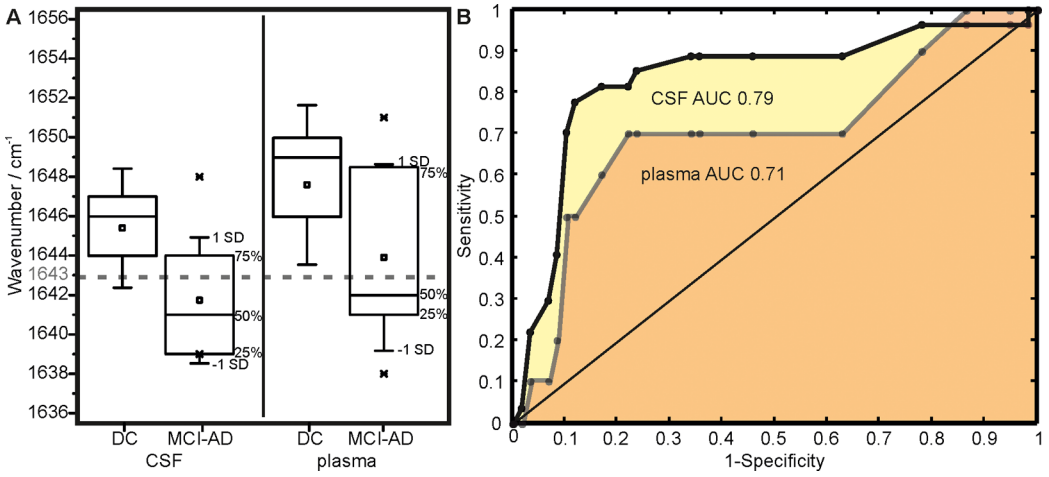

Figure 3. Distributions of the amide I maximum frequencies as recorded of CSF and plasma indicate a separable spectral downshift associated with MCI-AD progression (A). A marker band at 1643 cm^{-1} separates DC with 86% accuracy for CSF and 83% for plasma from (dashed line) MCI-AD. 25/50/75% quantiles are displayed in box-plots as horizontal lines, the average band position (square), ± standard deviation (whiskers), and observed minimum/maximum values (×) are displayed. A ROC curve was obtained by variation of the marker frequency (B). An AUC of 0.79 was achieved for CSF (yellow) and 0.71 for plasma (orange).

DOI: 10.1021/acs.analchem.5b04286
Anal. Chem. 2016, 88, 2755−2762

Table 2. (A) Summary of the Spectral Discrimination between Disease Control and DAT Samples of CSF and Blood, (B) Summary of the Spectral Discrimination between Disease Control and MCI-AD Samples, and (C) Additional Test Set Validation Results of the Marker Band Criterion for Disease Control and DAT Discrimination

A	accuracy %	sensitivity %	specificity %	AUC
CSF	90	94	88	0.9
EDTA-plasma	84	75	88	0.83

B	accuracy %	sensitivity %	specificity %	AUC
CSF	86	73	88	0.79
EDTA-plasma	83	50	88	0.71

C	accuracy %	sensitivity %	specificity %
CSF validation	90	88	93

significantly downshifted average amide I maximum at 1644 ± 5 cm^{-1} with the median at 1642 cm^{-1} ($p < 0.05$, Figure 3A). With the same marker band as used above, an accuracy of 83%, sensitivity of 50%, and a specificity of 88% for the discrimination between MCI-AD and DC were achieved based on the analysis of blood plasma (Table 2B). ROC-curve analysis yielded an AUC of 0.71 (Figure 3B).

In summary, the average amide I band positions of Aβ peptides in CSF and in plasma of MCI-AD patients were downshifted and might be predictive for AD before clinical symptoms appear.

CONCLUSIONS

The accumulation of amyloid in the brain of AD patients is a characteristic feature of Alzheimer's disease and starts years before cognitive decline manifests.[1−4] This suggests that Aβ peptides in CSF and blood samples of AD patients may show an increased level of misfolded states, especially of β-sheet enriched Aβ conformations.[5,44−46] Employing a novel immuno-IR-sensor, we confirm an increase of β-sheet rich soluble Aβ-conformations in CSF and blood of DAT patients. This was indicated by a spectral downshift of the secondary structure sensitive amide I band frequency. The observed downshift of the amide I marker band in DAT patients was inversely correlated with the decrease of Aβ1-42 in CSF. On the other hand, no correlation was found with the less amyloidogenic Aβ1-40. Moreover, the amide I band correlated positively with the tau protein concentration in CSF, which is considered a biomarker of neuronal damage. This supports the idea that pathological misfolding of Aβ is associated with neurotoxicity. However, the analysis of CSF samples with the novel immuno-IR-sensor revealed an accuracy of 90%, whereas the analysis of blood plasma yielded an accuracy of 84% for the identification of DAT patients (Table 2). Thus, the results obtained with the novel infrared-sensor using CSF and blood samples were in excellent agreement with the CSF-NDD supported clinical AD diagnosis.

The results obtained from CSF samples were validated using a limited, but independent sample set, indicating a prediction accuracy of 90%. More importantly, the deciding marker frequency appears to robustly distinguish the DAT and DC classes. The marker frequency 1643 cm^{-1} distinguished the available 130 CSF DAT and DC samples with an accuracy of 90%, a sensitivity of 92%, a specificity of 89%, and an ROC of 0.89 (Figure S-8).

Still, these findings have to be validated in a larger, independent clinical study. Interestingly, a similar spectral downshift was observed in CSF and blood of a small number of MCI-AD patients. The identical discriminative marker frequency, which was applied for clinically overt AD, separated the MCI-AD and DC group, however, with a reduced accuracy of approximately 83%. Therefore, the Aβ amide I band frequency appears to provide a highly promising novel biomarker candidate and our assay may identify AD at a predementia stage. The immuno-IR-sensor comprises several advantages: The label-free analysis does neither rely on the misfolding of a single, specific Aβ peptide species nor on the quantification of a specific soluble oligomeric form. In addition, our assay provides an intrinsic spectroscopic control of each preparative step. Thereby, preparative errors can be easily identified and subsequently avoided.

For optimum reproducibility of the results, we did not reuse sensors after partial removal of the surface functionalization. Naturally, a reusable sensor element would increase the analytical throughput. Methods for regeneration remain to be researched.

The sensor was constructed to fit into standard sized research spectrometers. However, advanced spectrometer setups, e.g., including quantum cascade lasers as thermal source, may increase the sensitivity.

Regarding the patient collective, our study is limited by a challenge bias (STARDdem criteria[38]) since only patients with predominantly early or prodromal AD have been investigated, and only patients with probable DAT were included (possible DAT excluded). Moreover, only patients were included whose diagnoses were cross-validated by CSF dementia biomarkers. Finally, patients attending an expert university memory clinic may not be representative for the general AD population.

Summing up, the application of an immuno-IR-sensor to measure the Aβ secondary structure distribution in CSF and blood plasma was demonstrated. Our novel findings indicate Aβ misfolding into β-sheet enriched conformations in body fluids of DAT and even MCI-AD patients. Using the sensor, excellent accuracies of 84−90% were obtained and validated. Thus, the secondary structure distribution of Aβ in CSF and blood provides a promising novel biomarker candidate to support the clinical diagnosis. Notably, these results were achieved with a single test and a single readout parameter. In general, the patients were phenotyped clinically and by well-established CSF dementia biomarkers (total-Tau, phospho-Tau, and the Aβ peptide ratio 1-42/1-40), which were measured by a single expert laboratory (P. Lewczuk, Erlangen). Like F18-Amyloid-PET, CSF guided neurochemical dementia diagnostics can be regarded as a state-of-the-art cross validation of the clinical AD diagnosis.

Follow-up studies are planned to (i) verify the findings in an independent cohort, to (ii) further evaluate the diagnostic potential with emphasis on preclinical stages, to (iii) research whether a combination of the amide I maximum position with one or more of the established biomarkers may further increase the accuracy of AD diagnosis, and to (iv) evaluate the potential of the technology to investigate the secondary structure distribution of other proteins known to be associated with neurodegenerative disorders like α-synuclein for Parkinson disease. Thus, the immuno-sensor may also support the biomarker guided diagnosis of other protein misfolding diseases, such as Parkinson disease, Parkinson dementia, dementia with Lewy bodies, subphenotypes of Frontotemporal

DOI: 10.1021/acs.analchem.5b04286
Anal. Chem. 2016, 88, 2755−2762

Lobar Degeneration, Chorea Huntington, and prion diseases. Furthermore, this sensor could potentially also be used to monitor the therapeutic efficacy of drug candidates which support the refolding of Aβ back to the less neurotoxic α-helical form.

■ ASSOCIATED CONTENT

Supporting Information

The Supporting Information is available free of charge on the ACS Publications website at DOI: 10.1021/acs.analchem.5b04286.

Schematic drawing of the immuno-IR-setup; reproducibility of the immuno-IR-sensor and evidence of Aβ extraction from CSF and blood by fluorescence spectroscopy; antibody A8978 did not induce a secondary structure change; Aβ monomers, oligomers and fibrils display different amide I maxima; increased β-sheet isoforms shift the amide I band of Aβ in disease control patients; correlation of AD biomarkers with the Aβ amide I maximum position; validation of the marker band criterion for DAT identification on CSF; table of summary of sample specifications; and phenotyping data of the sample collective and comparison of CSF and blood-plasma IR-analysis (PDF)

■ AUTHOR INFORMATION

Corresponding Author

*E-mail: gerwert@bph.rub.

Notes

The authors declare no competing financial interest.

[⊥]For questions regarding the clinical issues in the Supporting Information, please contact J.W. at jens.wiltfang@med.uni-goettingen.de.

■ ACKNOWLEDGMENTS

This research was supported by the Protein Research Unit Ruhr within Europe (PURE), Ministry of Innovation, Science and Research of North-Rhine Westphalia, Germany. A patent application was filed (WO 2015121339 A1). Further, this work was supported by the FP7 EU Grant NADINE (Grant Agreement Number 246513) and by the German Bundesministerium für Bildung und Forschung (Grant 01ED1203A) as a part of the BIOMARKAPD Project in the JPND Program.

■ REFERENCES

(1) Braak, H.; Braak, E. *Neurobiol. Aging* **1997**, *18* (4), 351−357.

(2) Price, J. L.; McKeel, D. W.; Buckles, V. D.; Roe, C. M.; Xiong, C.; Grundman, M.; Hansen, L. a.; Petersen, R. C.; Parisi, J. E.; Dickson, D. W.; Smith, C. D.; Davis, D. G.; Schmitt, F. a.; Markesbery, W. R.; Kaye, J.; Kurlan, R.; Hulette, C.; Kurland, B. F.; Higdon, R.; Kukull, W.; Morris, J. C. *Neurobiol. Aging* **2009**, *30* (7), 1026−1036.

(3) Jack, C. R.; Knopman, D. S.; Jagust, W. J.; Shaw, L. M.; Aisen, P. S.; Weiner, M. W.; Petersen, R. C.; Trojanowski, J. Q. *Lancet Neurol.* **2010**, *9* (1), 119−128.

(4) Jack, C. R.; Knopman, D. S.; Jagust, W. J.; Petersen, R. C.; Weiner, M. W.; Aisen, P. S.; Shaw, L. M.; Vemuri, P.; Wiste, H. J.; Weigand, S. D.; Lesnick, T. G.; Pankratz, V. S.; Donohue, M. C.; Trojanowski, J. Q. *Lancet Neurol.* **2013**, *12*, 207−216.

(5) Hardy, J. A.; Higgins, G. A. *Science (Washington, DC, U. S.)* **1992**, *256* (5054), 184−185.

(6) Drachman, D. A. *Alzheimer's Dementia* **2014**, *10* (3), 372−380.

(7) Cavallucci, V.; D'Amelio, M.; Cecconi, F. *Mol. Neurobiol.* **2012**, *45*, 366−378.

(8) Haass, C.; Selkoe, D. J. *Nat. Rev. Mol. Cell Biol.* **2007**, *8* (2), 101−112.

(9) World Health Organization and Alzheimer's Disease International. *Dementia: A Public Health Priority*; World Health Organization: Geneva, Switzerland, 2012.

(10) McKhann, G.; Drachman, D.; Folstein, M.; Katzman, R.; Price, D.; Stadlan, E. M. *Neurology* **1984**, *34* (7), 939−944.

(11) Dubois, B.; Feldman, H. H.; Jacova, C.; Dekosky, S. T.; Barberger-gateau, P.; Cummings, J.; Delacourte, A.; Galasko, D.; Gauthier, S.; Jicha, G.; Meguro, K.; Brien, J. O.; Pasquier, F.; Robert, P.; Rossor, M.; Salloway, S.; Stern, Y.; Visser, P. J.; Scheltens, P.; Pierre, U.; Paris, C.; Victor, U.; Bordeaux, S. *Lancet Neurol.* **2007**, *6*, 734−746.

(12) Jack, C. R.; Albert, M. S.; Knopman, D. S.; McKhann, G. M.; Sperling, R. A.; Carrillo, M. C.; Thies, B.; Phelps, C. H. *Alzheimer's Dementia* **2011**, *7* (3), 257−262.

(13) McKhann, G. M.; Knopman, D. S.; Chertkow, H.; Hyman, B. T.; Jack, C. R.; Kawas, C. H.; Klunk, W. E.; Koroshetz, W. J.; Manly, J. J.; Mayeux, R.; Mohs, R. C.; Morris, J. C.; Rossor, M. N.; Scheltens, P.; Carrillo, M. C.; Thies, B.; Weintraub, S.; Phelps, C. H. *Alzheimer's Dementia* **2011**, *7* (3), 263−269.

(14) Albert, M. S.; Dekosky, S. T.; Dickson, D.; Dubois, B.; Feldman, H. H.; Fox, N. C.; Gamst, A.; Holtzman, D. M.; Jagust, W. J.; Petersen, R. C.; Snyder, P. J.; Carrillo, M. C.; Thies, B.; Phelps, C. H. *Alzheimer's Dementia* **2011**, *7*, 270−279.

(15) Sperling, R. A.; Aisen, P. S.; Beckett, L. A.; Bennett, D. A.; Craft, S.; Fagan, A. M.; Iwatsubo, T.; Jack, C. R.; Kaye, J.; Montine, T. J.; Park, D. C.; Reiman, E. M.; Rowe, C. C.; Siemers, E.; Stern, Y.; Yaffe, K.; Carrillo, M. C.; Thies, B.; Morrison-Bogorad, M.; Wagster, M. V.; Phelps, C. H. *Alzheimer's Dementia* **2011**, *7* (3), 280−292.

(16) Price, J. L. *Neurobiol. Aging* **1997**, *18* (4 Suppl), S67−S70.

(17) Hampel, H.; Wilcock, G.; Andrieu, S.; Aisen, P.; Blennow, K.; Broich, K.; Carrillo, M.; Fox, N. C.; Frisoni, G. B.; Isaac, M.; Lovestone, S.; Nordberg, A.; Prvulovic, D.; Sampaio, C.; Scheltens, P.; Weiner, M.; Winblad, B.; Coley, N.; Vellas, B. *Prog. Neurobiol.* **2011**, *95* (4), 579−593.

(18) Mosconi, L.; Berti, V.; Glodzik, L.; Pupi, A.; Santi, S. De. *J. Alzheimers Dis.* **2010**, *20*, 843−854.

(19) Wang-Dietrich, L.; Funke, S. A.; Kühbach, K.; Wang, K.; Besmehn, A.; Willbold, S.; Cinar, Y.; Bannach, O.; Birkmann, E.; Willbold, D. *J. Alzheimers Dis.* **2013**, 985−994.

(20) Mapstone, M.; Cheema, A. K.; Fiandaca, M. S.; Zhong, X.; Mhyre, T. R.; MacArthur, L. H.; Hall, W. J.; Fisher, S. G.; Peterson, D. R.; Haley, J. M.; Nazar, M. D.; Rich, S. A.; Berlau, D. J.; Peltz, C. B.; Tan, M. T.; Kawas, C. H.; Federoff, H. J. *Nat. Med.* **2014**, *20* (4), 415−418.

(21) Schoonenboom, S. N. M.; Visser, P. J.; Mulder, C.; Lindeboom, J.; Van Elk, E. J.; Van Kamp, G. J.; Scheltens, P. H. *Neurocase* **2005**, *11* (1), 8−13.

(22) Hye, A.; Riddoch-Contreras, J.; Baird, A. L.; Ashton, N. J.; Bazenet, C.; Leung, R.; Westman, E.; Simmons, A.; Dobson, R.; Sattlecker, M.; Lupton, M.; Lunnon, K.; Keohane, A.; Ward, M.; Pike, I.; Zucht, H. D.; Pepin, D.; Zheng, W.; Tunnicliffe, A.; Richardson, J.; Gauthier, S.; Soininen, H.; Kłoszewska, I.; Mecocci, P.; Tsolaki, M.; Vellas, B.; Lovestone, S. *Alzheimer's Dementia* **2014**, *10*, 799−807.

(23) Gaugler, J. E.; Kane, R. L.; Johnston, J. A.; Sarsour, K. *Am. J. Alzheimer's Dis. Other Dementias* **2013**, *28* (4), 337−347.

(24) Sarroukh, R.; Cerf, E.; Derclaye, S.; Dufrêne, Y. F.; Goormaghtigh, E.; Ruysschaert, J. M.; Raussens, V. *Cell. Mol. Life Sci.* **2011**, *68* (8), 1429−1438.

(25) Cerf, E.; Sarroukh, R.; Tamamizu-Kato, S.; Breydo, L.; Derclaye, S.; Dufrêne, Y. F.; Narayanaswami, V.; Goormaghtigh, E.; Ruysschaert, J.-M.; Raussens, V. *Biochem. J.* **2009**, *421* (3), 415−423.

(26) Fändrich, M.; Meinhardt, J.; Grigorieff, N. *Prion* **2009**, *3* (2), 89−93.

(27) Sachse, C.; Fändrich, M.; Grigorieff, N. *Proc. Natl. Acad. Sci. U. S. A.* **2008**, *105* (21), 7462−7466.

(28) Glabe, C. G. *J. Biol. Chem.* **2008**, *283* (44), 29639−29643.

DOI: 10.1021/acs.analchem.5b04286
Anal. Chem. 2016, 88, 2755−2762

(29) Xia, W.; Yang, T.; Shankar, G.; Smith, I. M.; Shen, Y.; Walsh, D. M.; Selkoe, D. J. *Arch. Neurol.* **2009**, *66* (2), 417−428.
(30) Yang, T.; O'Malley, T. T.; Kanmert, D.; Jerecic, J.; Zieske, L. R.; Zetterberg, H.; Hyman, B. T.; Walsh, D. M.; Selkoe, D. J. *Alzheimer's Res. Ther.* **2015**, *7* (1), 1−16.
(31) Bruggink, K. a; Jongbloed, W.; Biemans, E. a L. M.; Veerhuis, R.; Claassen, J. a H. R.; Kuiperij, H. B.; Verbeek, M. M. *Anal. Biochem.* **2013**, *433* (2), 112−120.
(32) Nabers, A.; Ollesch, J.; Schartner, J.; Kötting, C.; Genius, J.; Haußmann, U.; Klafki, H.; Wiltfang, J.; Gerwert, K. *J. Biophoton.* **2015**, DOI: 10.1002/jbio.201400145.
(33) Kötting, C.; Gerwert, K. *ChemPhysChem* **2005**, *6* (5), 881−888.
(34) Ollesch, J.; Künnemann, E.; Glockshuber, R.; Gerwert, K. *Appl. Spectrosc.* **2007**, *61* (10), 1025−1031.
(35) Elfrink, K.; Ollesch, J.; Stöhr, J.; Willbold, D.; Riesner, D.; Gerwert, K. *Proc. Natl. Acad. Sci. U. S. A.* **2008**, *105*, 10815−10819.
(36) Frost, B.; Ollesch, J.; Wille, H.; Diamond, M. I. *J. Biol. Chem.* **2009**, *284* (6), 3546−3551.
(37) Wille, H.; Bian, W.; McDonald, M.; Kendall, A.; Colby, D. W.; Bloch, L.; Ollesch, J.; Borovinskiy, A. L.; Cohen, F. E.; Prusiner, S. B.; Stubbs, G. *Proc. Natl. Acad. Sci. U. S. A.* **2009**, *106* (40), 16990−16995.
(38) Noel-Storr, A. H.; McCleery, J. M.; Richard, E.; Ritchie, C. W.; Flicker, L.; Cullum, S. J.; Davis, D.; Quinn, T. J.; Hyde, C.; Rutjes, A. W. S.; Smailagic, N.; Marcus, S.; Black, S.; Blennow, K.; Brayne, C.; Fiorivanti, M.; Johnson, J. K.; Kopke, S.; Schneider, L. S.; Simmons, A.; Mattsson, N.; Zetterberg, H.; Bossuyt, P. M. M.; Wilcock, G.; McShane, R. *Neurology* **2014**, *83* (4), 364−373.
(39) American Psychiatric Association. *Diagnostic and Statistical Manual of Mental Disorders*, 4th ed.; The Association: Washington, DC, 1994.
(40) Lewczuk, P.; Esselmann, H.; Otto, M.; Maler, J. M.; Henkel, A. W.; Henkel, M. K.; Eikenberg, O.; Antz, C.; Krause, W. R.; Reulbach, U.; Kornhuber, J.; Wiltfang, J. *Neurobiol. Aging* **2004**, *25* (3), 273−281.
(41) Waedt, J.; Kleinow, M.; Kornhuber, J.; Lewczuk, P. *Biomarkers Med.* **2012**, *6*, 685−690.
(42) Lewczuk, P.; Zimmermann, R.; Wiltfang, J.; Kornhuber, J. *J. Neural Transm.* **2009**, *116* (9), 1163−1167.
(43) Schartner, J.; Güldenhaupt, J.; Mei, B.; Rögner, M.; Muhler, M.; Gerwert, K.; Kötting, C. *J. Am. Chem. Soc.* **2013**, *135* (10), 4079−4087.
(44) Karran, E.; Mercken, M.; Strooper, B. De. *Nat. Rev. Drug Discovery* **2011**, *10* (9), 698−712.
(45) Tanzi, R. E.; Bertram, L. *Cell* **2005**, *120*, 545−555.
(46) Kung, H. F. *ACS Med. Chem. Lett.* **2012**, *3*, 265−267.

DOI: 10.1021/acs.analchem.5b04286
Anal. Chem. 2016, 88, 2755−2762

Supplement

Amyloid-β-Secondary Structure Distribution in Cerebrospinal Fluid and Blood Measured by an Immuno-IR-Sensor: A Biomarker Candidate for Alzheimer's Disease

Andreas Nabers[1], Julian Ollesch[1], Jonas Schartner[1], Carsten Kötting[1], Just Genius[2], Henning Hafermann[2], Hans Klafki[3], Klaus Gerwert[1]* and Jens Wiltfang[2,3,4]

[1]Department of Biophysics, Faculty of Biology and Biotechnology, Ruhr-University Bochum, Germany

[2]Clinics for psychiatry and psychotherapy, LVR-clinical center Essen, Germany

[3]Department of Psychiatry and Psychotherapy, University Medical Center (UMG), Georg-August-University Göttingen, Germany

[4]German Center for Neurodegenerative Diseases (DZNE), Grisebachstraße 5, 37077 Göttingen, Germany

*Corresponding author: Klaus Gerwert

Correspondence for the immuno-sensor: Klaus Gerwert (gerwert@bph.rub.de)
Correspondence for clinical issues: Jens Wiltfang (jens.wiltfang@med.uni-goettingen.de)

Table of contents:

Detection and analysis of Aβ in CSF and blood

The immuno-IR-sensor-setup consists of a conventional FTIR-spectrometer (Bruker Vertex 70v), a peristaltic pump, and a flow-through cuvette, which is implemented into the sample compartment of the spectrometer (Figure S-1). A special feature of the flow-through cuvette is the internal reflection element (IRE, Germanium), wherein the incoming infrared beam gets totally reflected multiple times and attenuated by interaction with the sample. Thereby, the sample is pumped (one-way or circulating) with a constant flow-rate of 1 ml/min by a peristaltic pump.

The principle of the sensor was recently reported [1].

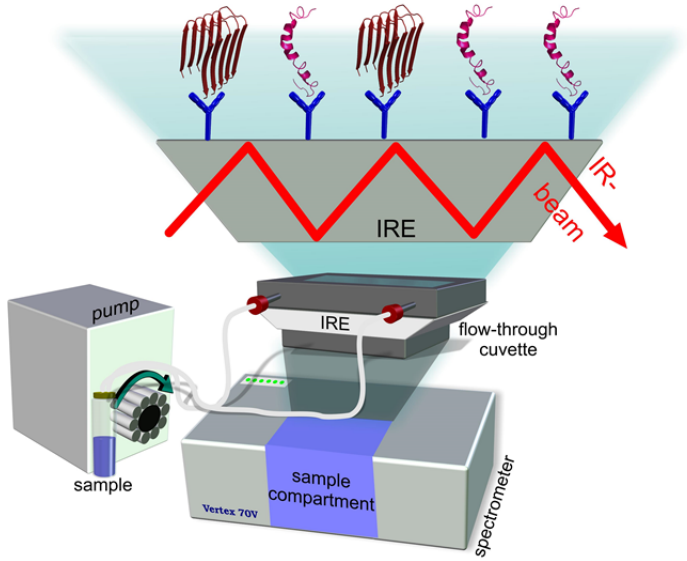

Figure S-1. Schematic drawing of the immuno-IR-sensor-setup. An ATR-flow-through cuvette is implemented into a conventional FTIR-spectrometer. The sample is pumped by a peristaltic pump through the flow-through cuvette and proteins of interest can be immobilized on the antibody functionalized sensor surface. Thus, only specific biomarker candidates can be analyzed regarding their secondary structure distribution in the respective body fluid.

In the original version, monoclonal antibody (mAb) 1E8 against an N-terminal epitope of Aβ was used as the capture antibody [1]. As it turned out, the FTIR-spectra recorded from Aβ in CSF and EDTA blood plasma were not reproducible. Major differences were observed between repeated measurements of the same CSF sample, particularly in the amide I band (Figure S-2A).

In the current, improved version of the sensor, the monoclonal Antibody 1E8 was replaced by monoclonal antibody A8978 (Sigma Aldrich). A8978 provided reproducible performance and recorded a characteristic amide I maximum presumably reflecting an average from all Aβ-variants present in the sample (Figure S-2C).

No binding of human serum albumin, α-synuclein or IgG_2 immunoglobulin was observed (Figure S-2D). Further, the reproducibility of each single procedural step, antibody functionalization and blocking, was demonstrated (Figure S-2E). The reproducibility of the surface silanization was published in [2]. Fluorescence measurements were performed to confirm Aβ extraction from CSF and blood plasma by the antibody functionalized sensor surface. Therefore, after capture of Aβ peptides with A8978, the sensor was probed with CF™ 633 labeled 1E8 antibody. As control, the same was done in the absence of Aβ on the surface. No fluorescence signal was observed in the control experiment (Figure S-3AI, AIII). In contrast, after capturing Aβ peptides from CSF or blood plasma, fluorescence was detected confirming Aβ capture by antibody A8978 (Figure S-

3AII, AIV). The intensity of the signal was about 7 times higher in CSF than in blood plasma, which correlates with a lower Aβ concentration in blood (Figure S-3BI, BII).

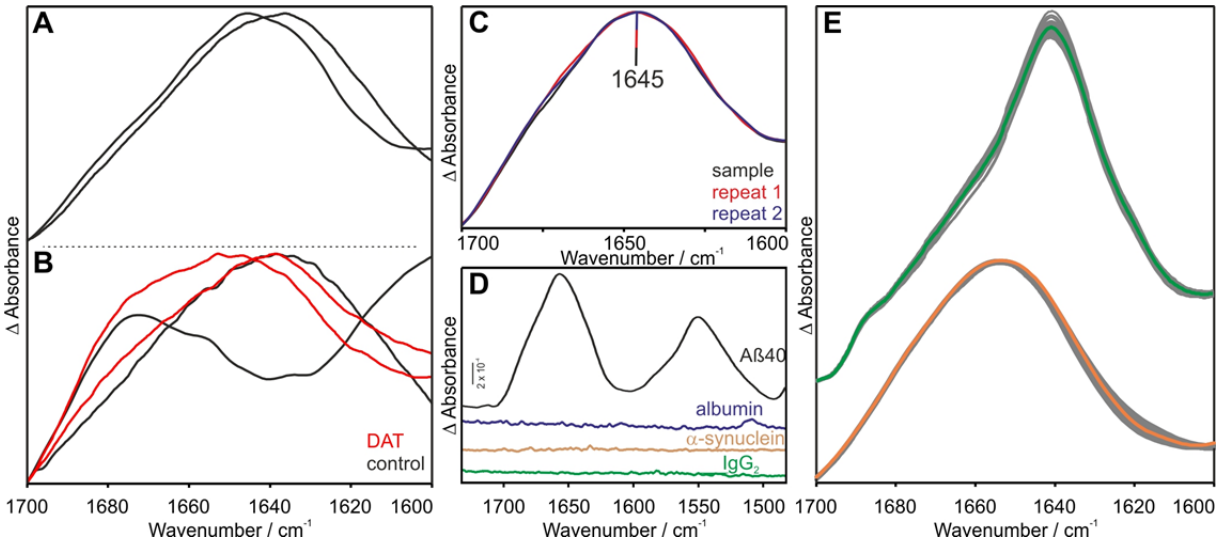

Figure S-2. Repeated Aβ analysis with one CSF sample using two sensor elements prepared with mAb 1E8 showed differences of the recorded amide I bands (A). Thus, a differentiation between two non-neurodegenerative disease control and two DAT patients was not possible (B). Contrastingly, detection with mAb A8978 was highly reproducible, as demonstrated with the repeated analysis of one CSF sample with three sensors (C). Further, A8978 did neither bind albumin (HSA), immunoglobulins or alpha-synuclein (D). The method reproducibility of different measurements was shown for the antibody functionalizing (E; n=25, mean spectrum in green) and the blocking step (E; n=10, mean spectrum in orange). Reproducibility of the silanization step was tested in [2].

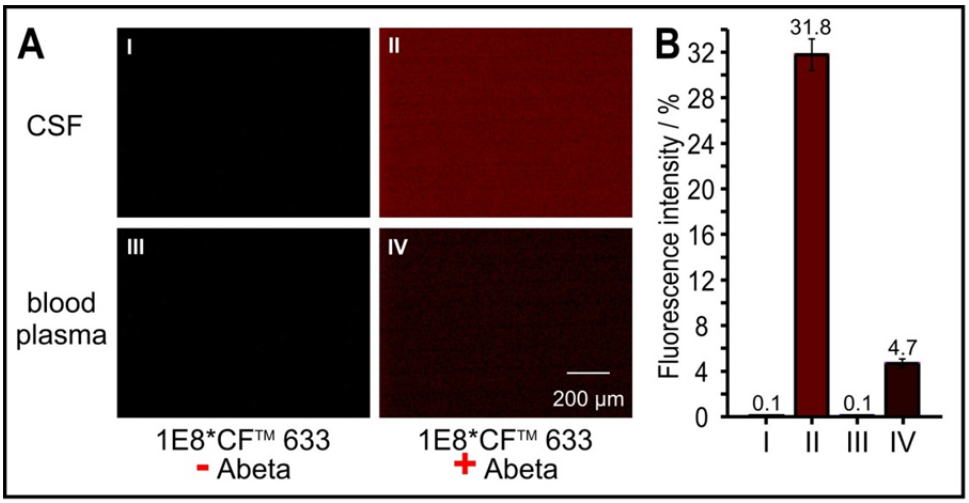

Figure S-3. Evidence for Aβ binding to the sensor surface. The mAb A8978 (Aß13-23) was used as primary capture antibody receptive for Aβ from CSF and blood. Fluorescence detection was performed with mAb 1E8 labeled with CF™ 633 (A) and fluorescence intensity of buffer rinsed surfaces was recorded (B). In the absence of Aβ, the labeled mAb 1E8 did not bind to the surface (AI, AIII, BI, BIII). A more intense fluorescence signal was observed with CSF (AII, BII) than with blood plasma (AIV, BIV).

Antibody binding did not induce a secondary structure change

The protein characteristic amide I band did not change in its shape or maximum during incubation for 60 min and subsequent rinsing for 20 min of the ATR-FTIR sensor (Figure S-4). Thus, the antibody A8978 did not induce a secondary structural change during Aβ binding over time.

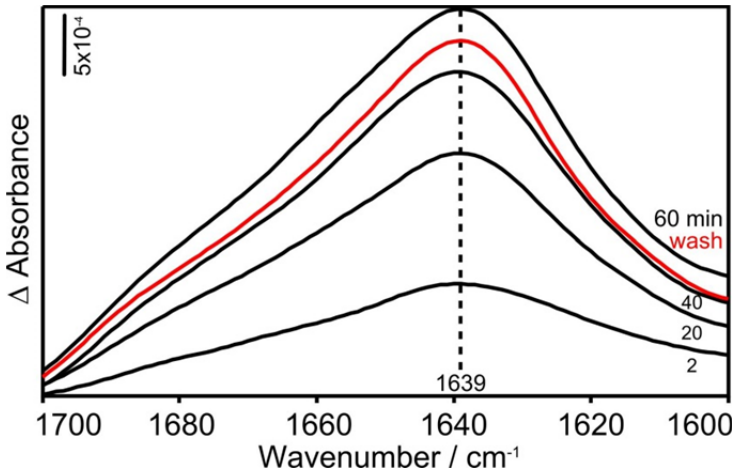

Figure S-4. The amide I band of Aβ extracted out of a DAT CSF sample did not change its characteristic shape and maximum absorbance peak during binding to the antibody A8978. Thus, no secondary structural changes were observed during 60 min incubation (black) and after 20 min of buffer rinsing (red).

Aβ monomers, oligomers and fibrils display different amide I maxima

The internal reflection element of the ATR-FTIR-sensor was chemically functionalized with mAb A8978. The sensor produced signals with pure solutions of synthetic Aβ1-42 monomers, oligomers and fibrillar forms. Each displayed a characteristic amide I maximum (Figure S-5A-D). The recorded infrared absorbance spectra of Aβ from complex liquid samples represent an integrated signal of all Aβ species and conformations. The more β-sheet enriched Aβ conformations contribute to the integrated IR-spectrum, the more the amide I band maximum becomes downshifted. This effect is demonstrated *in silico* with a modeled amide I band calculated as a linear combination of scaled amide I bands recorded from monomeric, oligomeric and fibrillary Aβ1-42 and Aβ1-40. An increase of the soluble, β-sheet rich oligomeric fraction shifts the maximum band position to a lower wavenumber (Figure S-5E), as long as the β-sheet rich conformation does not represent the majority of the sample. This extreme condition cannot generally be expected in natural body fluids.

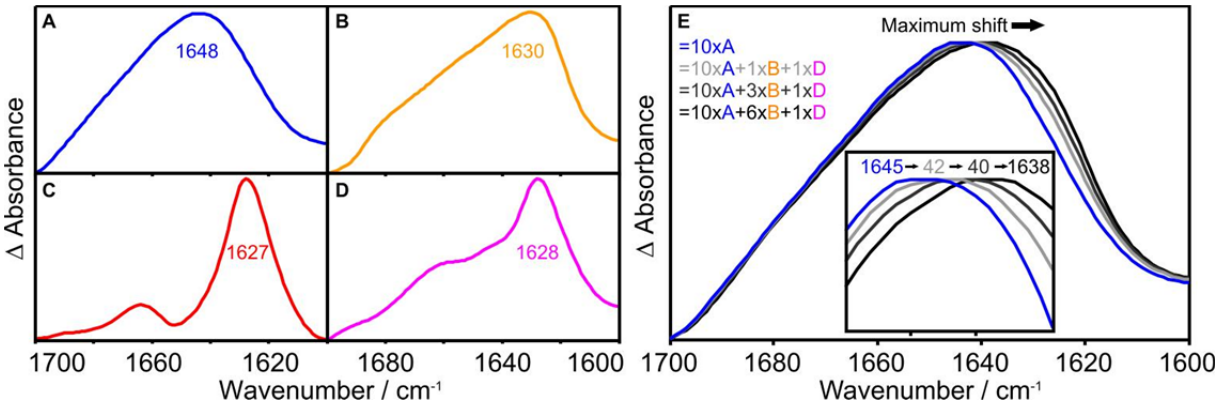

Figure S-5. The antibody A8978 recognizes Aβ monomers, oligomers and fibrills independently from their secondary structures. Hence, A8978 extracted synthetic Aβ1-42 monomers (A), Aβ1-42 oligomers (B), fibrillar Aβ1-42 (C), and fibrillary Aβ1-42 forms out of pure solutions. The maxima of the amide I bands are highlighted in color. Scaled linear combinations of (A-C) with increasing fractions of particularly the oligomeric compound (B) shift the maximum frequency towards lower wavenumbers (E).

However, the amide I band of Aβ extracted from a disease control CSF sample shifted to lower wavenumbers by adding low quantities of synthetic Aß fibrils (1 ng/ml) to the immobilized fraction, leading to an increase of β-sheet isoforms in the respective fluid as expected in Alzheimer's disease patients (Figure S-6). The amide I band shifted from 1648 cm^{-1} to 1641 cm^{-1}. Consequently, a lower content of β-sheet enriched Ab isoforms in the respective fluid may result in a minor maximum shift. But, a spectral downshift can be interpreted by an increase of β-sheet isoforms in body fluids of DAT patients.

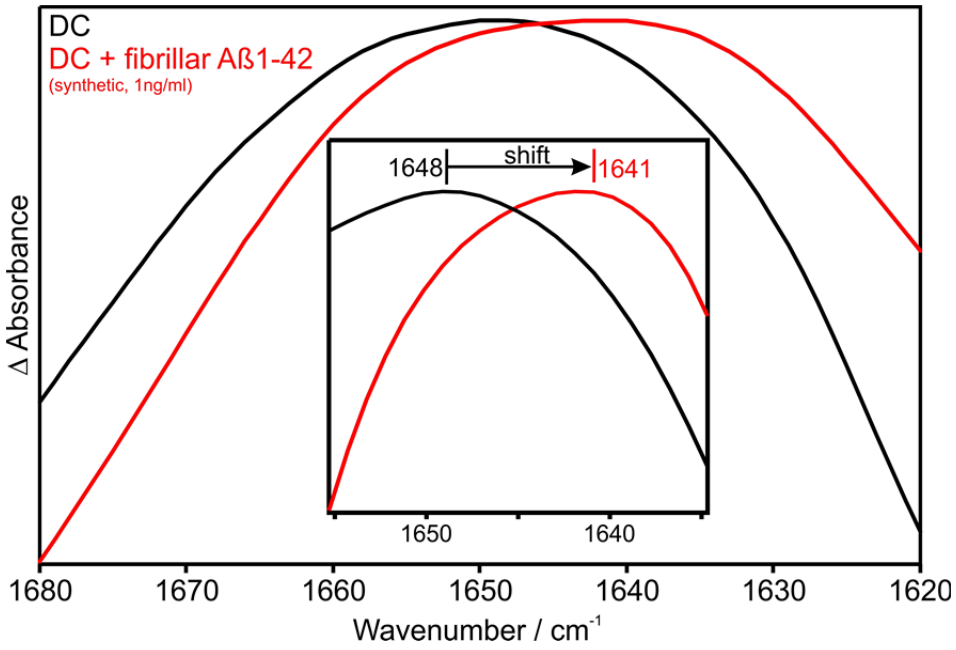

Figure S-6. The amide I band of Aβ extracted from CSF of a disease control patient (black) shifted to lower wavenumbers by adding 1 ng/ml synthetic fibrillar Aβ peptides to the surface-immobilized fraction. Thus, a spectral downshift can be interpreted by an increase of β-sheet isoforms in body fluids of DAT patients.

Preparation of monomeric, oligomeric and fibrillary Aβ peptides

First, Lyophilised synthetic Aβ1-42 (Bachem AG, Bubendorf, Switzerland) was dissolved in hexafluoroisopropanol (HFIP) at a concentration of 2 mg/ml over night at room temperature, and partitioned into 100 µg aliquots. HFIP was removed during 60 min in a centrifugal evaporator (Concentrator plus, Eppendorf, Hamburg, Germany) at RT and 20 mbar and subsequently stored until further use.

The protein film was dissolved in phosphate buffer (50 mM Na_2HPO_4/NaH_2PO_4, pH=8) and vortexed until a clear solution was obtained. For the analysis of monomeric Aβ, the solution was analyzed within 1 h after protein suspension in aqueous buffer.

Oligomers of Aβ1-42 were generated by HFIP-suspended monomers (2 mg/ml) diluted to 10 % HFIP in distilled water. Peptides were incubated for 15 min at RT and subsequently centrifuged for 15 min at 13000 g. The supernatant was further used and remaining HFIP was evaporated through a gentle N_2 stream for 1 h. Finally, the retentate of a 100 kDa centrifuge concentrator (Merck) was used. We determined the concentration of oligomerized peptides by UV spectrometry at 280 nm [3].

A fibril suspension was started with monomerized peptide. After dissolving the protein in buffer, the solution was incubated at 37 °C, shaking at 350 rpm (Thermomixer, Eppendorf) for at least 24 h. Fibrils were harvested by 30 min centrifugation at 13000 g, discarding the supernatant, and gentle resuspension of the pellet in PBS buffer. Protein concentrations were verified spectrometrically [3].

Aβ1-40 peptides (VCP Bio, Shenzhen City, China) were processed identically.

Correlation of AD biomarkers with the Aß amide I maximum position

In the next step, we compared the IR-marker frequency at 1643 cm^{-1} with the CSF level of Aβ1-42, the Aβ 42/40 ratio and the CSF-concentrations of ptau or ttau. It should be noted that these values had been considered for the diagnosis. In Figure S-5, the Aβ amide I band marker band at 1643 cm^{-1} is plotted against the different biomarkers. The 1643 cm^{-1} marker frequency of the amide I band is compared with the threshold values for Aβ1-42 (Figure S-7A), the Aβ 42/40 ratio (Erlangen) (Figure S-7B) ptau (Figure S-7C) and ttau (Figure S-7D). It spans the area highlighted in red, indicating the overlap of the marker assignments for DAT (Figure S-7A-D). Based on the area from Aβ1-42 and the amide I maximum position, an accuracy of 83 %, sensitivity of 53 % and specificity of 98 % were determined. In the same order, for the combination of the Aβ 42/40 ratio and the amide I maximum values of 92 %, 78 % and 98 % were obtained. Further, we received values of 94 %, 91 % and 95 % for the ttau/amide I maximum cluster. The best value was obtained for the combination with ptau. Based on this area, an improved accuracy of 96 %, specificity of 97 % and sensitivity of 94 % was calculated for the discrimination between disease control (DC) and DAT. In the present study, these biomarker cut-offs were used for AD diagnosis, thus the interpretation of these data for diagnostic purposes would lead to incorporation bias at this point. As impression for the future, the amide I maximum of Aβ in combination with ptau can be used as a novel biomarker for AD diagnosis.

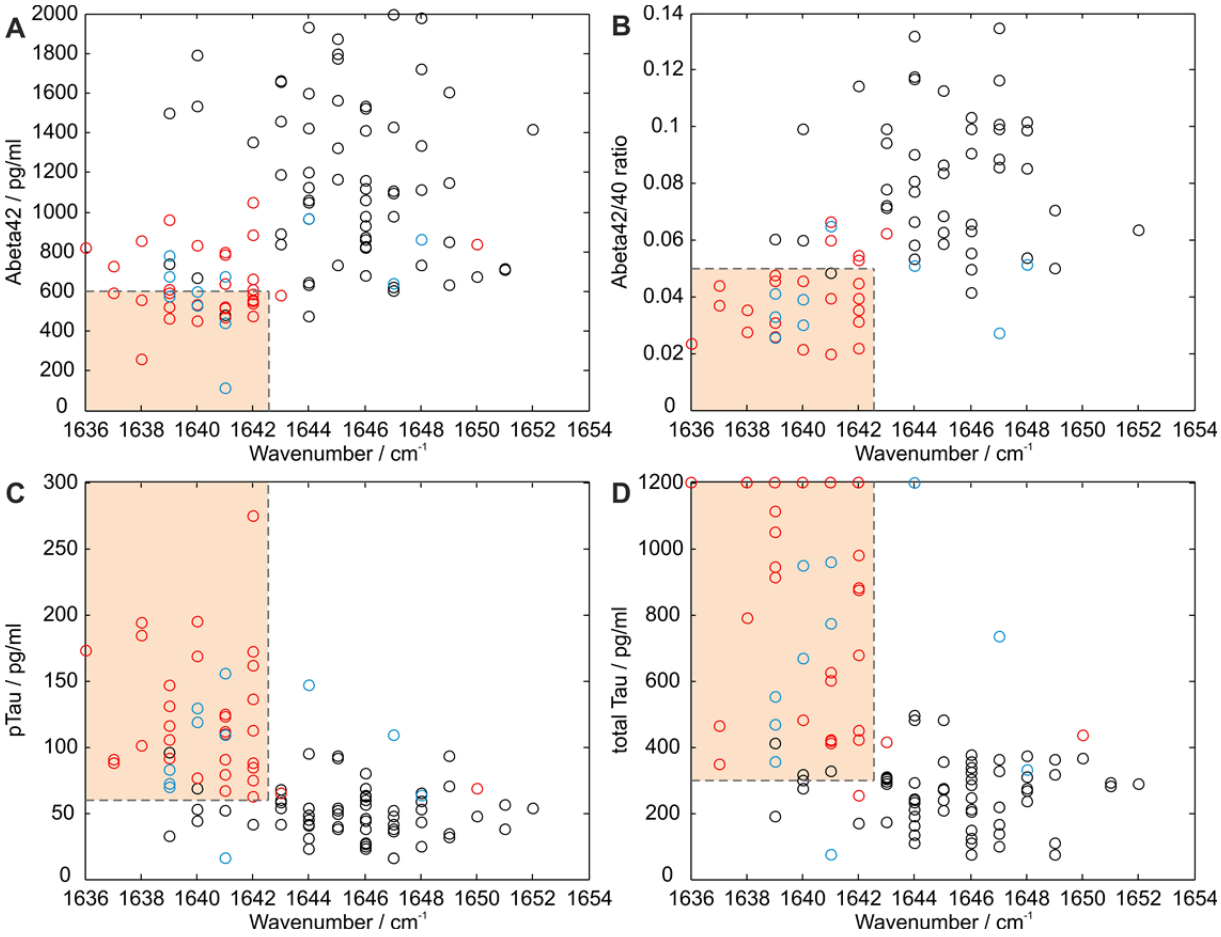

Figure S-7. Combination of CSF biomarker concentrations with the amide I maximum position of disease control (black circles), DAT (red circles) and MCI-AD (blue circles) patient CSF samples. The threshold of the amide I maximum frequency (1643 cm^{-1}) combined with neurochemical CSF biomarker cut off values (dashed lines) generate an area (red orange area) indicative for clinical DAT. Thus, an accuracy of 85 %, 91 %, 96 % and 94 % was achieved by combining the amide I maximum position with Aβ1-42 concentration (A) the Aβ 42/40 ratio (B) ptau (C) and the ttau protein concentration (D) in CSF.

Validation of the marker band criterion for DAT identification on CSF

The primary analyzed patient collective comprised 110 CSF samples, partitioned in 66 DC, 33 DAT, and 11 MCI-AD patients. The diagnostic potential of the immuno-IR-method for the discrimination between DC and DAT subjects was indicated by a prediction accuracy of 90 %, sensitivity of 94 %, and specificity of 88 % for CSF. Additionally, 31 CSF samples (14 DC, 17 DAT) could be recruited within this study and used for validation of the marker band criterion. Therefore, Aß was extracted from CSF as described before and the marker band criterion (<1643 cm^{-1} denotes DAT) was applied to the validation dataset. As a result, 14 DC and 17 DAT patients could be separated with an accuracy of 90 %, sensitivity of 88 %, and specificity of 93 % (Table 2C). The amide I distribution of Aβ is shown in Figure S-8A. Almost perfectly, the amide I maximum frequency distribution of the validation set matches the distribution of the primary collective (Figure S-8A) as presented in the manuscript (Figure 2A),

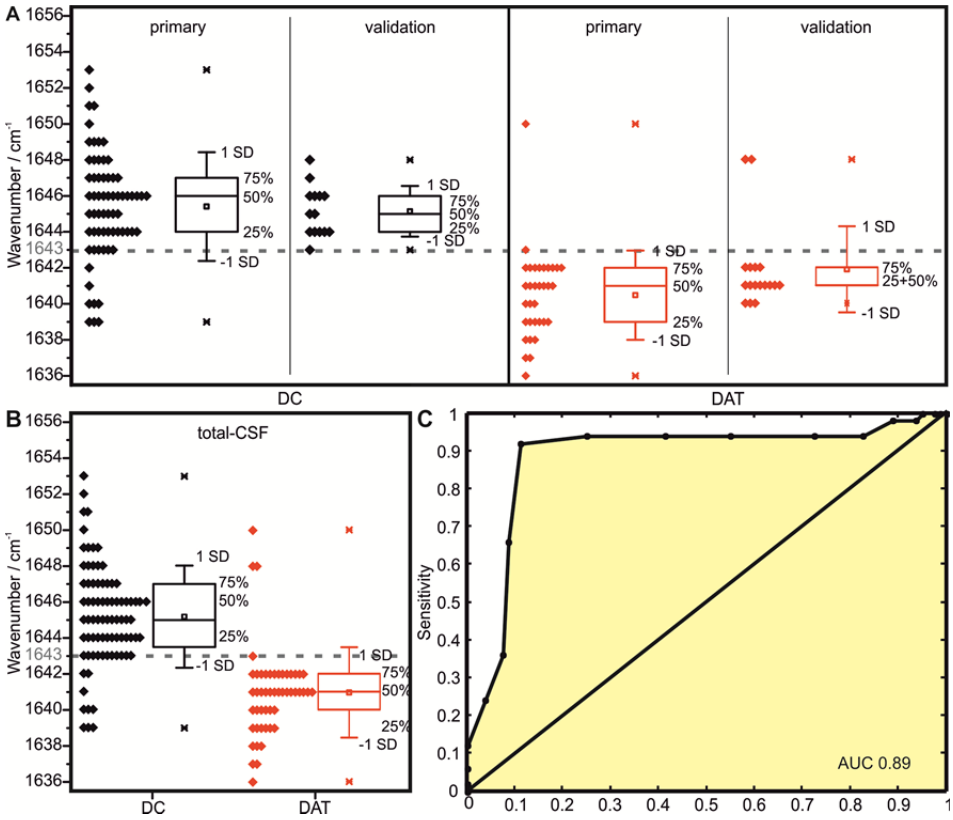

Figure S-8. The distributions of the amide I maximum frequencies as recorded from CSF of the primary patient collective (see Figure 2, 99 patients) and the validation collective (31 patients).indicate a clearly separable spectral downshift associated with DAT (A). Both the primary and the validation collective shows a similar amide I maximum distribution. The marker band criterion (<1643 cm^{-1} denotes DAT, dashed lines) separates controls and DAT patients of the validation set with an accuracy of 90 % (A). Black diamonds depict DC patient samples, red diamonds DAT cases. 25/50/75 % quantiles are displayed in box-plots as horizontal lines, the average band position (square), ± standard deviation (whiskers), and observed minimum/maximum values (x) are displayed. Moreover, the marker frequency distinguished the total-CSF sample collective (130 patients, 80 DC and 50 DAT) with an accuracy of 90 % (B). An AUC of 0.89 was achieved with CSF of the total patient collective.

The amide I maximum distribution of Aβ of the total-CSF sample collective is shown in Figure S-8B. Using the marker band criterion, as described above, the DC group could be separated from the DAT cases with an accuracy of 90 %, sensitivity of 92 %, and specificity of 89 %. Moreover, an AUC of 0.89 was achieved with CSF of the total patient collective. In summary, the validation results indicated that the marker band at 1643 cm^{-1} for DC and DAT discrimination appears to be a simple and robust biomarker.

Study participants

Table S-1. Summary of sample specifications of the primary (A, results see Manuscript) and the validation dataset (B).

A	Male	Female
age	67 ± 11	70 ± 12
AD	∑ 33	
	10	23
DC	∑ 66	
	33	33
MCI-AD	∑ 11	
	3	8
total #	46	64

B	Male	Female
age	81 ± 6	77 ± 8
AD	∑ 17	
	3	14
DC	∑ 14	
	3	11
total #	6	25

Comparison of CSF and blood-plasma analysis

Table S-2. Phenotyping data of the patient collective, including the dementia biomarkers and the amide I maximum position of the Aβ fraction in CSF and blood plasma of DC (A), DAT (B) and MCI-AD patients (C). Cutoff-values for DAT diagnosis are marked in italics.

A Patient number	Age	Sex (m/f)	MMSE *(27-30=cognitive unimpaired, 20-26=mild dementia, 10-19=moderate dementia, <10=severe dementia)*	Aß42 [pg/ml] *<600*	Aß42/40 ratio *<0.05*	MSD ratio Aß42/40 <0.0635	ptau [pg/ml] *>60*	ttau [pg/ml] *>300*	Amide I CSF [cm^{-1}] *<1643*	Amide I plasma [cm^{-1}] *<1643*
1	67	m	29	n.a.	n.a.	0,114	46	211	1646	1653
2	87	m	12	n.a.	n.a.	0,050	69,1	339	1646	1644
3	80	f	30	n.a.	n.a.	0,113	34,5	<75	1649	1649
4	52	m	30	n.a.	n.a.	0,128	26,6	<75	1646	1650
5	62	m	28	n.a.	n.a.	0,119	<15,6	100	1647	1652
6	80	m	n.a.	n.a.	n.a.	0,076	57	292	1651	1655
7	66	f	25	n.a.	n.a.	0,068	69	318	1640	1641
8	58	m	28	n.a.	n.a.	0,119	31,8	111	1649	1648
9	56	f	6	n.a.	n.a.	0,080	47,7	368	1650	1650
10	80	m	20	n.a.	n.a.	0,083	53,6	214	1644	1650
11	87	f	19	n.a.	n.a.	0,075	38,4	281	1651	1650
12	67	f	21	11042	0,099	0,127	36,1	165	1647	1649
13	62	m	n.a.	15795	0,055	0,087	38	206	1646	n.a.
14	56	f	n.a.	17150	0,116	0,112	48,1	218	1647	1646
15	42	f	n.a.	n.a.	n.a.	0,118	63,8	247	1646	1644
16	70	f	28	n.a.	n.a.	0,109	22,5	112	1646	1646
17	57	m	25	8067	0,132	0,110	23,4	109	1644	1650
18	68	m	26	18111	0,099	0,111	44,2	275	1640	1651

19	65	m	n.a.	9973	0,049	0,048	52,4	327	1641	1650
20	68	m	23	12032	0,054	0,044	94,8	483	1644	1645
21	57	f	n.a.	16752	0,099	0,119	42,3	174	1643	1639
22	62	f	24	17637	0,081	0,112	49,3	190	1644	1648
23	89	f	16	<800	n.a.	0,057	41,8	233	1644	n.a.
24	82	f	20	10985	0,101	0,107	38,3	220	1647	1643
25	74	m	24	>40000	n.a.	0,074	58	311	1643	1644
26	74	f	25	16647	0,072	0,072	65,4	308	1643	1647
27	55	m	27	20752	0,087	0,120	92,3	356	1645	1646
28	60	m	30	15504	0,099	0,120	80,2	303	1646	1650
29	67	m	27	22886	0,050	0,080	92,8	363	1649	1649
30	69	m	29	22312	0,064	0,127	54,4	289	1652	1638
31	83	f	n.a.	12510	0,066	0,072	43,7	286	1646	1652
32	54	f	29	27330	0,069	0,130	52,4	276	1645	1646
33	60	m	30	4489	0,135	0,123	<15,6	140	1647	1649
34	71	m	10	11585	0,090	0,102	45,3	243	1644	1651
35	53	f	28	n.a.	n.a.	0,110	n.a.	n.a.	1653	1649
36	82	m	28	11754	0,113	0,120	39,7	242	1645	1646
37	92	f	20	10676	0,068	0,068	49,6	273	1645	1652
38	77	f	20	13544	0,054	0,065	53,3	275	1648	1649
39	70	f	n.a.	30213	0,059	0,126	93,1	481	1645	1649
40	61	m	29	16132	0,089	0,119	42,1	328	1647	1650
41	85	f	n.a.	22687	0,071	0,123	71,3	316	1649	1648
42	50	f	22	18664	0,084	0,121	37,5	209	1645	1648
43	63	f	30	20141	0,072	0,098	53,6	296	1643	1652
44	75	m	24	22395	0,042	0,060	62,9	355	1646	1652
45	79	f	13	11380	0,086	0,100	52,1	364	1647	1648
46	66	f	13	10951	0,102	0,114	25,2	267	1648	1651
47	51	m	26	15604	0,086	0,119	42,8	238	1648	1637
48	78	f	29	25582	0,060	0,120	53,1	299	1640	1651
49	78	m	27	>33000	n.a.	0,085	96,2	412	1639	1643
50	60	m	n.a.	27506	0,058	0,111	48,9	162	1644	1649
51	44	f	27	16772	0,091	0,121	25,1	126	1646	1646
52	88	f	21	22433	0,050	0,099	57,2	378	1646	n.a.
53	81	f	13	13667	0,063	0,084	60,3	325	1646	1649
54	84	f	n.a.	11194	0,103	0,125	27,7	150	1646	1648
55	83	m	25	20051	0,099	0,115	65	374	1648	n.a.
56	71	m	27	16524	0,117	0,113	53,6	292	1644	1653
57	70	f	28	18593	0,063	0,064	54,2	272	1645	1642
58	58	f	29	14571	0,067	0,062	49,1	495	1644	n.a.
59	61	m	n.a.	11442	0,078	0,104	59,5	291	1643	1649
60	74	m	28	17551	0,094	0,118	68,4	305	1643	1639
61	65	m	26	9568	0,118	0,107	40,8	239	1644	n.a.
62	66	m	29	17441	0,099	0,097	59,2	311	1648	n.a.
63	44	m	30	11812	0,114	0,107	41,8	169	1642	1640
64	69	f	27	15551	0,077	0,108	31,1	134	1644	1643
65	75	m	n.a.	n.a.	n.a.	0,113	n.a.	n.a.	1639	1650
66	58	f	n.a.	12308	0,060	0,105	33,3	190	1639	n.a.
mean	68		24	16707	0,082	0,100	50,5	262	1645	1648
SD ±	12		6	7038	0,023	0,023	18,7	96	3	4
min value	42		6	<800	0,042	0,044	<15,6	<75	1639	1637
max value	92		30	>40000	0,135	0,130	96,2	495	1653	1655
B										
67	78	m	22	837	n.a.	0,060	69,1	436	1650	1654
68	79	f	19	261	n.a.	0,038	185	>1200	1638	n.a.
69	61	m	25	455	0,021	0,040	169	>1200	1640	1650
70	59	f	n.a.	534	n.a.	0,051	195	>1200	1640	1651

71	79	f	22	525	n.a.	0,043	123	600	1641	1637
72	81	f	19	640	n.a.	0,063	79,1	414	1641	1641
73	69	f	21	587	n.a.	0,031	275	>1200	1642	1640
74	57	m	16	541	0,055	0,070	62,8	256	1642	1641
75	55	f	22	558	0,028	0,060	101	790	1638	1643
76	79	m	18	561	0,022	0,059	74,5	450	1642	1650
77	58	m	17	664	n.a.	0,042	162	980	1642	1640
78	73	f	20	596	0,044	0,046	87,7	349	1637	1641
79	56	f	n.a.	593	0,048	0,056	106	914	1639	1638
80	79	f	16	963	0,046	0,063	147	1050	1639	1641
81	78	f	n.a.	582	0,062	0,062	64,5	417	1643	1641
82	86	f	19	643	0,060	0,059	90,6	420	1641	1638
83	58	f	25	856	0,036	0,045	194	>1200	1638	1639
84	85	m	n.a.	819	0,024	0,045	173	>1200	1636	1641
85	79	f	17	522	0,031	0,040	91,7	944	1639	1642
86	78	m	12	888	0,039	0,055	113,4	877	1642	1642
87	75	f	23	612	n.a.	0,051	115,8	1114	1639	1638
88	72	f	12	n.a.	n.a.	0,051	n.a.	n.a.	1639	1640
89	68	f	n.a.	464	0,026	0,037	131	>1200	1639	1638
90	72	m	22	787	0,039	0,061	112	>1200	1641	1641
91	78	f	24	515	n.a.	0,043	110	627	1641	1645
92	87	f	22	610	0,045	0,049	172	>1200	1642	n.a.
93	69	f	10	832	0,046	0,058	76,9	482	1640	1646
94	65	m	16	1052	0,053	0,067	84,9	424	1642	1639
95	79	f	24	801	0,066	0,059	66,6	423	1641	n.a.
96	92	f	24	551	0,031	0,034	136	882	1642	1638
97	68	m	15	728	0,037	0,050	91,1	465	1637	1641
98	51	f	25	474	0,035	0,054	88	680	1642	n.a.
99	68	f	24	469	0,020	0,039	125	>1200	1641	n.a.
mean	72		20	641	0,040	0,051	121,0	812	1640	1642
SD ±	10		4	171	0,014	0,010	48,9	341	2	4
min value	51		10	261	0,020	0,031	62,8	256	1636	1637
max value	92		25	1052	0,066	0,070	275,0	>1200	1643	1651
C										
100	55	m	27	439	n.a.	0,039	156	959	1641	1643
101	71	f	26	597	0,039	0,053	119	950	1640	1641
102	73	f	26	675	0,033	0,052	72,2	355	1639	n.a.
103	67	f	26	530	0,030	0,034	129	667	1640	1644
104	70	m	27	577	0,026	0,039	69,5	469	1639	1641
105	52	f	30	860	0,051	0,056	64,3	331	1648	1650
106	60	f	29	638	0,027	0,037	109	735	1647	1641
107	62	f	27	782	0,041	0,052	82,7	554	1639	1651
108	67	m	27	970	0,051	0,051	147	>1200	1644	1650
109	70	f	26	675	0,065	0,044	109	772	1641	1640
110	76	f	27	116	n.a.	0,043	15,6	<75	1641	1638
mean	66		27	624	0,044	0,045	97,6	642	1642	1644
SD ±	8		1	226	0,013	0,008	41,3	327	3	5
min value	52		26	116	0,026	0,034	15,6	<75	1639	1638
max value	76		30	970	0,065	0,056	156,0	>1200	1648	1651

References

[1] Nabers A, Ollesch J, Schartner J, Kötting C, Genius J, Haußmann U, et al. An infrared sensor analysing label-free the secondary structure of the Abeta peptide in presence of complex fluids. J Biophotonics 2015;9999:n/a – n/a. doi:10.1002/jbio.201400145.

[2] Schartner J, Güldenhaupt J, Mei B, Rögner M, Muhler M, Gerwert K, et al. Universal method for protein immobilization on chemically functionalized germanium investigated by ATR-FTIR difference spectroscopy. J Am Chem Soc 2013;135:4079–87. doi:10.1021/ja400253p.

[3] Gill SC, von Hippel PH. Calculation of protein extinction coefficients from amino acid sequence data. Anal Biochem 1989;182:319–26.